Tellurium quantum dots: Preparation and optical properties

Cite as: Appl. Phys. Lett. **111**, 063112 (2017); https://doi.org/10.1063/1.4993819
Submitted: 01 July 2017 . Accepted: 31 July 2017 . Published Online: 11 August 2017

Chaoyu Lu, Xueming Li, Libin Tang, Sin Ki Lai, Lukas Rogée, Kar Seng Teng, Fuli Qian, Liangliang Zhou, and Shu Ping Lau

Tellurium quantum dots: Preparation and optical properties

Chaoyu Lu,[1] Xueming Li,[1,a)] Libin Tang,[2,b)] Sin Ki Lai,[3] Lukas Rogée,[3] Kar Seng Teng,[4] Fuli Qian,[1] Liangliang Zhou,[1] and Shu Ping Lau[3]
[1]*Key Laboratory of Advanced Technique & Preparation for Renewable Energy Materials, Ministry of Education, Yunnan Normal University, Kunming 650500, People's Republic of China*
[2]*Kunming Institute of Physics, Kunming 650223, People's Republic of China*
[3]*Department of Applied Physics, The Hong Kong Polytechnic University, Hong Kong, People's Republic of China*
[4]*College of Engineering, Swansea University, Bay Campus, Fabian Way, Swansea SA1 8EN, United Kingdom*

(Received 1 July 2017; accepted 31 July 2017; published online 11 August 2017)

Herein, we report an effective and simple method for producing Tellurium Quantum dots (TeQDs), zero-dimensional nanomaterials with great prospects for biomedical applications. Their preparation is based on the ultrasonic exfoliation of Te powder dispersed in 1-methyl-2-pyrrolidone. Sonication causes the van der Waals forces between the structural hexagons of Te to break so that the relatively coarse powder breaks down into nanoscale particles. The TeQDs have an average size of about 4 nm. UV-Vis absorption spectra of the TeQDs showed an absorption peak at 288 nm. Photoluminescence excitation (PLE) and photoluminescence (PL) are used to study the optical properties of TeQDs. Both the PLE and PL peaks revealed a linear relationship against the emission and excitation energies, respectively. TeQDs have important potential applications in biological imaging and catalysis as well as optoelectronics. *Published by AIP Publishing.*
[http://dx.doi.org/10.1063/1.4993819]

Since the discovery of low-dimensional materials, extensive studies have shown that the properties of these materials altered significantly when they are in the nanoscale regime. For example, a low-dimensional material can exhibit unique mechanical, electrical, or optical properties that are different from those of their bulk counterparts. Quantum dots (QDs), the lowest-dimensional materials, are no exception to that, and they could be engineered to display a wide range of properties that appear to be attractive for many modern fields of study.

Quantum dots (QDs) with diameters typically smaller than 10 nm have attracted much research interest in recent years due to their possible applications in biomedicine, such as photothermal therapy for cancer cell ablation and bioimaging.[1–4] The optical properties of QDs are indispensable factors in deciding over their suitability for these applications.[5–7] For example, lasers with a wavelength of ~800 nm are commonly used in photothermal therapy as they allow penetration of the biological tissues, such as skin, to reach cancer cells inside the bodies.[8–10] On the other hand, the photoluminescence quantum yield is an important factor for bioimaging applications.[11,12] As a result, the studies of the optical properties of various QDs have gained increasing attention. The optical properties of QDs are different from those of their respective bulk materials due to the significant quantum confinement in all spatial dimensions.[13] The bandgap increases due to the confined electron waves, which affects both the optical absorption and the photoluminescence wavelength to a large extent. Therefore, it is of great scientific interest to investigate the optical properties of various QDs so as to pave the way for potential biomedical applications.

In this work, tellurium quantum dots (TeQDs) were prepared by ultrasonic ablation of Te bulk powder and dispersed in solvent. After purification, X-ray diffraction (XRD), transmission electron microscopy (TEM), scanning electron microscopy (SEM), and atomic force microscopy (AFM) were used to study their structural and morphological properties, and X-ray photoelectron microscopy (XPS) and energy dispersive spectroscopy (EDS) were used to investigate their chemical composition and bonding. This was followed by systematic determination of the optical properties of the TeQDs to investigate their optical absorption and PL.

Te powder (99.999%) and 1-Methyl-2-pyrrolidone (NMP) were purchased from Sinopharm Chemical Reagent Co., Ltd. All chemicals were used as received without further purifications.

0.5 g of Te powder was ground into fine powder in an agate mortar and was then transferred into a beaker, and 50 ml of NMP was added. The solution was sonicated for 4 h in an ultrasonic bath at room temperature. The resultant dark brown suspension was centrifuged at 2000 rpm for 15 min. The clear and brown-colored supernatant was collected as TeQD solution.

The morphology, size distribution, and crystal structure of the TeQDs were investigated using TEM (Tecnai G2 TF30 S-Twin). The diameter of the TeQDs was further confirmed using AFM (Seiko SPA 400). The XRD (Ultima IV, X-ray source: Cu Kα, $\lambda = 0.154178$ nm) of TeQDs was performed for comparison with bulk Te to ensure the structural integrity of TeQDs after ultrasound treatment. The chemical bonding was analyzed by XPS (PHI Versa probe II) using 50 W Al Kα radiation. Optical absorption was performed using a UV-Vis spectrometer (Shimadzu UV-3600). PL measurements were carried out using a fluorescence spectrometer (Hitachi, F-4500).

a)E-mail: lxmscience@163.com
b)E-mail: scitang@163.com

The lattice of tellurium is a long chain structure. The atoms are covalently bonded to form long helical chains that are spatially arranged in parallel through the van der Waals effect. Due to the weak van der Waals forces, TeQDs were obtained after grinding, ultrasonic treatment, and centrifugation of the Te powder. Figure 1(a) shows the TeQDs dispersed in the solution.

Figure 1(b) shows the TEM image of the TeQDs. The TeQDs have a dot-like shape and diameter below 10 nm. The TeQDs have a narrow size distribution ranging from 3 to 5 nm as shown in Fig. 1(c). It fits well with a Gaussian distribution (red line), which implied that the TeQDs formed a monodispersion. The fitting parameters indicated that the average diameter of TeQDs was 4.10 nm with a small FWHM of 0.9 nm. The good crystallinity of the TeQDs was revealed in the high resolution TEM (HR-TEM) image shown in Fig. 1(d).[14] The lattice fringes were clearly identified with a lattice interplanar distance of 0.172 nm as seen from the line profile (blue line) in Fig. 1(e), which corresponded to the (102) plane of tellurium. The SEM image of the TeQD film formed from repeated drop-casting of TeQD solution followed by solvent evaporation is shown in Fig. 1(f). EDS performed on the film as shown in Fig. 1(g) revealed that the atomic ratio of C/N/O/Te was 26.4/6.9/26.2/40.5 (%). C, N, and O could originate from the NMP solvent adsorbing water molecules from air, which possibly indicated the oxidation of TeQDs to TeO_2 by oxygen from the air, as reported by Garbassi *et al.*[15]

Figure 1(i) shows the XRD pattern of the TeQD film. The peaks at $2\theta = 27.56°$, 38.26°, and 40.41° corresponded to the (101), (102), and (110) lattice planes of tellurium, respectively. The peak of (101) has the largest intensity and represents a *d*-spacing of 0.323 nm [Fig. 1(h)]. The XRD pattern was in good agreement with the trigonal tellurium (*t*-Te). The average particle size in the TeQD film was calculated using the Debye-Scherrer equation

$$D = 0.89\lambda/(\beta \cos\theta), \tag{1}$$

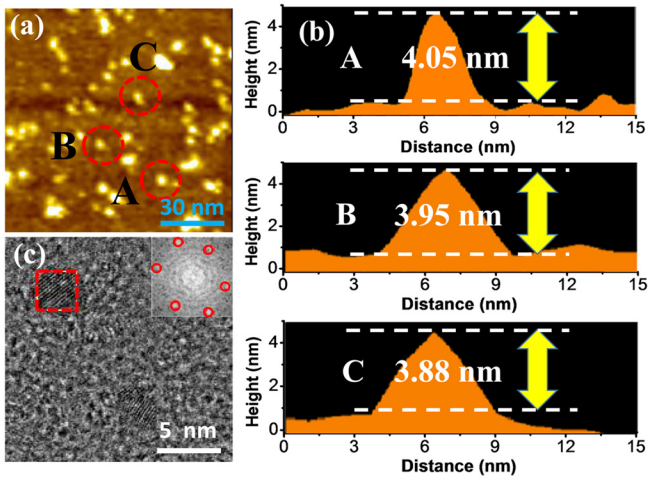

FIG. 2. (a) AFM image of the TeQDs. (b) The height analysis of locations A, B, and C indicated in (a). (c) The HR-TEM image of the TeQDs; inset: the Fast Fourier Transform (FFT) of the selected TeQD.

where *D* is the average particle size, λ is the X-ray wavelength, and β and θ are the FWHM (= 0.357 nm) and diffraction angle of the (101) peak, respectively. The average particle size obtained from Eq. (1) was 3.96 nm, which is consistent with the average size of TeQDs observed from the TEM measurement.

The AFM measurement was also performed to determine the size of the TeQDs. The AFM image of the TeQDs is shown in Fig. 2(a). The height profiles of three TeQDs labeled with A, B, and C are shown in Fig. 2(b), and their heights were 4.05, 3.95, and 3.88 nm respectively, with an average height of 3.96 nm. This was consistent with the TEM and XRD measurements.

The bandgap energy (E_g) of TeQDs was calculated using[16]

$$E_g \approx E_{g(0)} + \frac{\hbar^2\pi^2}{2\mu R^2} - \frac{1.78e^2}{\varepsilon R}. \tag{2}$$

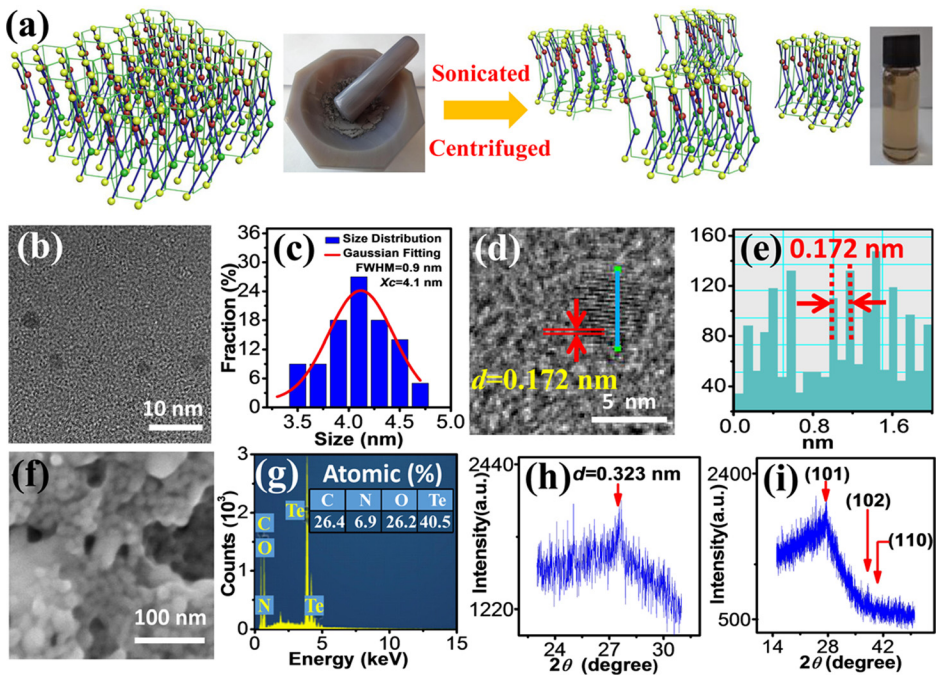

FIG. 1. (a) The schematic illustration of the preparation of TeQDs. (b) TEM image of TeQDs. (c) Particle size distribution of TeQDs from TEM. (d) The HR-TEM image of one TeQD. (e) The line profile analysis of TeQD. (f) The SEM image of the TeQD film. (g) The EDS analysis of the TeQD film. (h) The XRD diffraction pattern of TeQDs. (i) The full scan XRD diffraction pattern of the TeQDs.

Here, $E_{g(0)}$ is the bandgap of bulk Te (0.35 eV),[17] $\hbar$ ($\hbar = h/(2\pi)$) is the reduced Planck constant, e is the electron charge, μ ($\mu = \left[\frac{1}{m_{e^-}} + \frac{1}{m_{h^+}}\right]^{-1}$) is the reduced mass of the electron and hole in the quantum region, ε ($\varepsilon = 5$) is the dielectric constant of Te, and R (2 nm) is the radius of TeQD. The calculated E_g value is 1.34 eV which is much larger than the bulk value (0.35 eV)[17] due to quantum effects.

The crystal structure of the TeQDs was investigated using fast Fourier transform (FFT) [see the inset in Fig. 2(c)] performed on the TeQDs indicated by a red square in Fig. 2(c). The FFT image showed that the TeQDs have a hexagonal crystal structure which was similar to the bulk tellurium. The hexagon in the FFT image was slightly tilted, which corresponded to the trigonal tellurium.

Figure 3(a) shows the Raman spectrum of the TeQDs. Two peaks appeared at 122.6 and 142.2 cm^{-1}, which could be attributed to the Te-Te bond vibrational modes.[18] When compared to the peak positions of 121.0 and 140.8 cm^{-1} reported for bulk tellurium by Vinod *et al.*,[18] the observed peaks for TeQDs were right-shifted by 1.6 and 1.4 cm^{-1}, respectively, which might indicate the presence of stress in the lattice of the TeQDs.[19] The shift towards higher frequencies could be related to the surface effect. As the diameter of the tellurium reduces, the surface area and surface energy would increase drastically.

The XPS spectrum of the TeQDs is presented in Fig. 3(b). The three strongest peaks located at 283.2, 574.5, and 583.8 eV were assigned to C 1s, Te $3d_{5/2}$, and Te $3d_{3/2}$ respectively. Two smaller peaks at 398 and 530 eV were the N 1s and O 1s peaks, respectively. The peaks marked with red arrows, such as the C 1s, N 1s, and O 1s peaks, were attributed to the NMP solvent and possible oxidation of Te forming TeO_2, as previously discussed. The two Te-related peaks, as shown in Fig. 3(c), were the Te $3d_{5/2}$ and Te $3d_{3/2}$ peaks. They were due to the spin-orbit coupling that led to a split of the Te 3d orbital.[20]

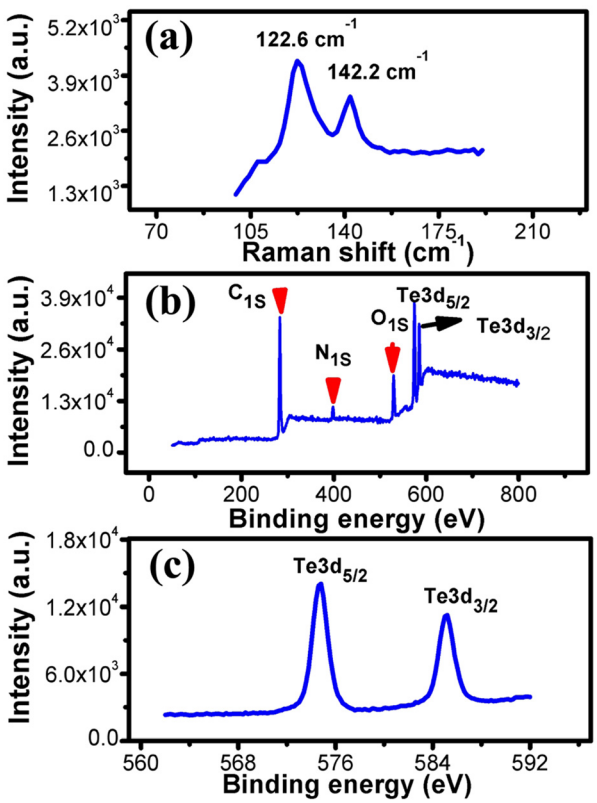

FIG. 3. (a) The Raman spectrum of the TeQDs. (b) The XPS spectrum of the TeQDs. (c) The Te $3d_{5/2}$ and Te $3d_{3/2}$ XPS spectra.

Figure 4(a) shows the UV-Vis absorption spectrum of the TeQD solution. The solution was gradually diluted in order to observe the absorption peak more clearly. An absorption peak was observed at 288 nm. The inset in Fig. 4(a) shows the photograph of the TeQD solution under ambient light (left) and ultraviolet light illumination (right).

The bandgap energy (E_g) of TeQDs can also be obtained by the Tauc plot using

$$\alpha h\nu = A(h\nu - E_g)^{1/2}, \tag{3}$$

where α is the absorption coefficient, A is a constant, $h\nu$ is the photon energy, and E_g is the bandgap energy. The bandgap energy of TeQDs[21] may be estimated from the curve of $(\alpha h\nu)^2$ *vs.* photo energy ($h\nu$), and the estimated value is 1.32 eV (as shown in Fig. S1 in the supplementary material) which is very near to that calculated from the quantum size effect (1.34 eV) using Eq. (2).

The photoluminescence (PL) spectra of the TeQD solution are shown in Fig. 4(b). The excitation wavelength was varied from 300 to 500 nm, in 20 nm steps. The excitation wavelength covered the range from UV to visible light. The PL emission of the TeQDs was basically within the visible light region between blue to green emission. As the excitation wavelength red-shifted, the emission peak also red-shifted, and thus, the TeQD solution exhibited excitation-wavelength-dependent emission, which was commonly observed in other QD solutions such as the graphene QDs.[20] The emission light energy is smaller than the excited energy, which is due to the vibrational relaxation caused by the Stokes shift.[22] The photoluminescence excitation (PLE) spectra are shown in Fig. 4(c). The peak marked with a star was due to the PLE system and not the sample. The emission intensity was monitored from 380 to 500 nm, in 20 nm steps. Similar to the PL emission spectra, the maximum PLE peak also red-shifted as the emission wavelength red-shifted. This is indicated with a black arrow. However, the peak at 263 nm did not shift with the emission wavelength as depicted by the red arrow. Based on the study on the structure and optical properties, the energy level structure has been proposed (as shown in Fig. S2 in the supplementary material), where only those photon energies that match specific energy level differences can be absorbed.[22] It is proposed that TeQDs contain multiple energy levels due to the quantum-size, which facilitates some electron transition pathways, leading to the red-shift of PL.

To investigate the wavelength-dependent PLE and PL peaks in greater detail, the normalized PLE and PL spectra are shown in Figs. 5(a) and 5(b), respectively. As the monitored emission wavelength (PLE) was red-shifted by 120 nm [Fig. 5(a)], the excitation wavelength that produced maximum emission (i.e., the PLE peak) also red-shifted by 43 nm. As the excitation wavelength red-shifted by 200 nm

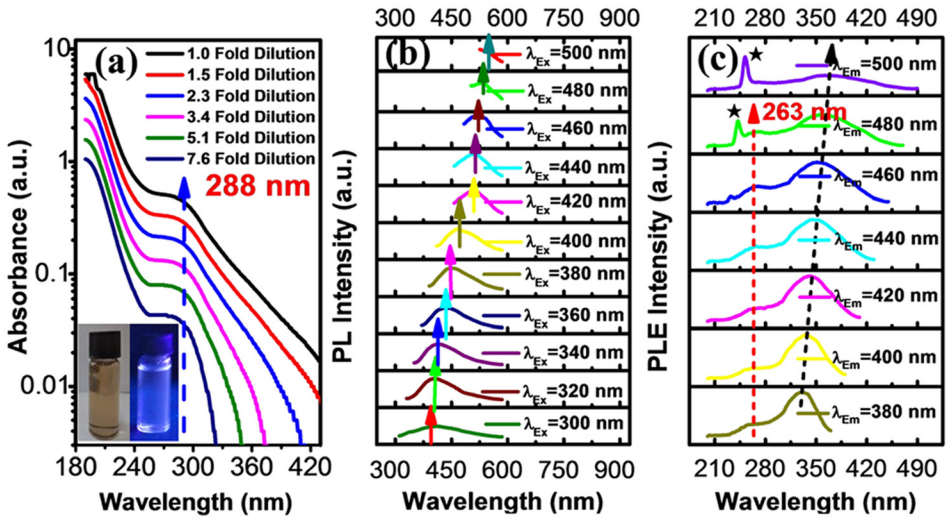

FIG. 4. (a) The UV-Vis absorption spectra of the TeQDs with different folds of dilution. (b) PL spectra of the TeQDs with excitation wavelengths ranging from 300 to 500 nm. (c) PLE spectra of the TeQDs recorded as a function of emission wavelength ranging from 380 to 500 nm.

[Fig. 5(b)], the emission wavelength (PL) also red-shifted by 151 nm. It was found that both the energy-dependence PLE and PL peaks followed closely a linear relationship as shown in Fig. 5(c). The linear dependence of PLE and PL peaks on energy enables multicolour emission properties, which enriches a variety of PL emission colours of TeQDs.

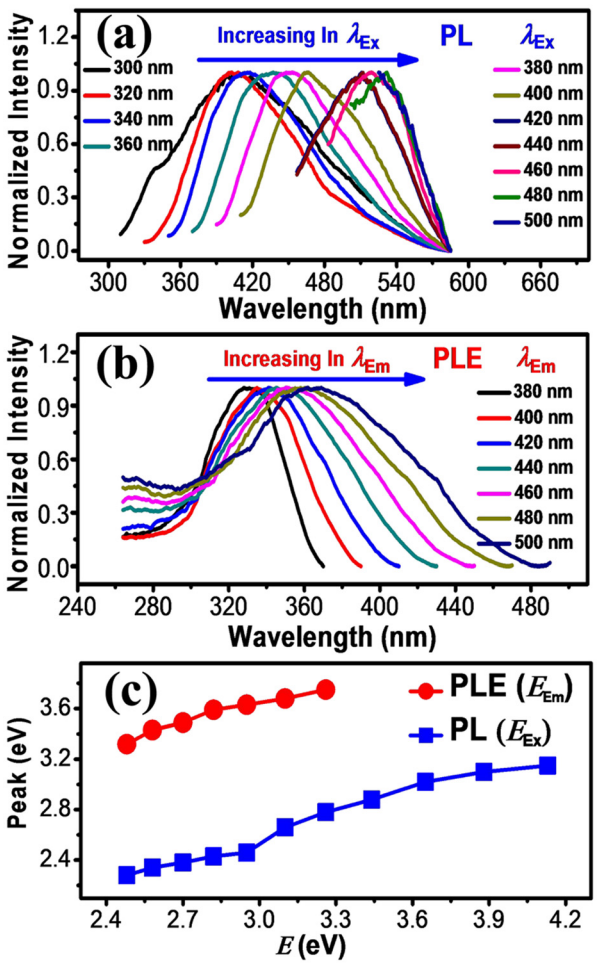

FIG. 5. (a) Normalized PL spectra of the TeQDs excited by various wavelengths ranging from 300 to 500 nm in 20 nm steps. (b) Normalized PLE spectra of the TeQDs. (c) The linear relationship between the peak excitation energy (PLE peak) and emission energy (E_{Em}, red line) and the linear relationship between the emission peak energy (PL peak) and excitation energy (E_{Ex}, blue line).

Tellurium quantum dots (TeQDs) with an average diameter of 4 nm were prepared by ultrasonic ablation of Te bulk powder. The as-prepared TeQDs have a narrow size distribution. The optical properties of the TeQDs including absorption and PL were investigated. The TeQDs absorbed strongly in the UV region, and the PL emission was in the visible light region with a wavelength tunable from the blue to green color by changing the excitation wavelength from 300 to 500 nm. The TeQDs have potential applications in photothermal therapy and bioimaging; however, its biocompatibility requires further investigation.

See supplementary material for the Tauc plot (supplementary Fig. S1) and the energy level diagram of TeQDs (supplementary Fig. S2).

This work was supported by the National Natural Science Foundation of China (Grant Nos. 51462037 and 61106098) and the Key Project of Applied Basic Research of Yunnan Province, China (Grant No. 2012FA003).

[1]R. Gui, H. Jin, Z. Wang, and L. Tan, Coord. Chem. Rev. **296**, 91 (2015).
[2]M. Chu, X. Pan, D. Zhang, Q. Wu, J. Peng, and W. Hai, Biomaterials **33**, 7071 (2012).
[3]M. Werwie, N. Fehr, X. Xu, T. Basché, and H. Paulsen, Biochim. Biophys. Acta **1840**, 1651 (2014).
[4]E. V. Shashkov, M. Everts, E. I. Galanzha, and V. P. Zharov, Nano Lett. **8**, 3953 (2008).
[5]S. V. Kershaw, A. S. Susha, and A. L. Rogach, Chem. Soc. Rev. **42**, 3033 (2013).
[6]J. Z. Zhang, J. K. Cooper, and S. Gul, J. Phys. Chem. Lett. **5**, 3694 (2014).
[7]C. S. S. Sandeep, J. M. Azpiroz, W. H. Evers, S. C. Boehme, I. Moreels, S. Kinge, L. D. A. Siebbeles, I. Infante, and A. J. Houtepen, ACS Nano **8**, 11499 (2014).
[8]B. del Rosal, E. Carrasco, F. Ren, A. Benayas, F. Vertrone, F. Sanz-Rodríguez, D. Ma, Á. Juarranz, and D. Jaque, Adv. Funct. Mater. **26**, 6060 (2016).
[9]A. Benayas, F. Ren, E. Carrasco, V. Marzal, B. del Rosal, B. A. Gonfa, Á. Juarranz, F. Sanz-Rodríguez, D. Jaque, J. Garía-Solé, D. Ma, and F. Vetrone, Adv. Funct. Mater. **25**, 6650 (2016).
[10]Y. Yong, X. Cheng, T. Bao, M. Zu, L. Yan, W. Yin, C. Ge, D. Wang, Z. Gu, and Y. Zhao, ACS Nano **9**, 12451 (2015).
[11]Z. Fan, Y. Li, X. Li, L. Fan, S. Zhou, D. Fang, and S. Yang, Carbon **70**, 149 (2014).
[12]L. Lin, Y. Xu, S. Zhang, I. M. Ross, A. C. M. Ong, and D. A. Allwood, ACS Nano **7**, 8214 (2013).
[13]C. Dong, X. Li, and J. Qi, Phys. Chem. Chem. Phys. **13**, 14476 (2011).

[14]Y. L. Wang, K. Yang, H. Q. Pan, S. Y. Liu, X. M. Xu, and L. Y. Zhou, Chem. J. Chin. Univ. **33**, 2604 (2012).
[15]F. Garbassi, J. C. J. Bart, and G. Petrini, J. Electron. Spectrosc. Relat. Phenom. **22**, 95 (1981).
[16]N. Satoh, T. Nakashima, K. Kamikura, and K. Yamamoto, Nat. Nanotech. **3**, 106 (2008).
[17]Z. H. Lin, Z. Yang, and H. T. Chang, Cryst. Growth Des. **8**, 351 (2008).
[18]E. M. Vinod, A. K. Singh, R. Ganesan, and K. S. Sangunni, J. Alloys Compd. **537**, 127 (2012).
[19]G. Lucovsky, Phys. Stat. Sol. **49**, 633 (1972).
[20]X. Li, S. Lau, L. Tang, R. Ji, and P. Yang, Nanoscale **6**, 5323 (2014).
[21]L. Ma, W. H. Li, and J. H. Luo, Mater. Lett. **102–103**, 65 (2013).
[22]X. Li, S. Lau, L. Tang, R. Ji, and P. Yang, J. Mater. Chem. C **1**, 7308 (2013).